

Swin3D++: Effective Multi-Source Pretraining for 3D Indoor Scene Understanding

Yu-Qi Yang^{1*} Yu-Xiao Guo² Yang Liu^{2†}

¹Tsinghua University ²Microsoft Research Asia

{t-yuqyan, yuxgu, yangliu}@microsoft.com

Abstract

Data diversity and abundance are essential for improving the performance and generalization of models in natural language processing and 2D vision. However, 3D vision domain suffers from the lack of 3D data, and simply combining multiple 3D datasets for pretraining a 3D backbone does not yield significant improvement, due to the domain discrepancies among different 3D datasets that impede effective feature learning. In this work, we identify the main sources of the domain discrepancies between 3D indoor scene datasets, and propose SWIN3D++, an enhanced architecture based on SWIN3D for efficient pretraining on multi-source 3D point clouds. SWIN3D++ introduces domain-specific mechanisms to SWIN3D’s modules to address domain discrepancies and enhance the network capability on multi-source pretraining. Moreover, we devise a simple source-augmentation strategy to increase the pretraining data scale and facilitate supervised pretraining. We validate the effectiveness of our design, and demonstrate that SWIN3D++ surpasses the state-of-the-art 3D pretraining methods on typical indoor scene understanding tasks. Our code and models will be released at <https://github.com/microsoft/Swin3D>.

1. Introduction

Point clouds are a common representation of 3D data, and extracting point-wise features from them is crucial for many 3D understanding tasks. Deep learning methods have achieved impressive results and progress in this domain, but they often require large and diverse datasets to improve feature learning. This is a common strategy in natural language processing and 2D vision, and it has also proven to be effective in enhancing model performance and generalizability in 3D vision [38, 45, 52, 48]. However, 3D data is much more

scarce and less annotated than image and text data, which poses significant challenges and limitations for the development and impact of 3D pretraining.

A straightforward solution to mitigate the data scarcity problem is to merge multiple existing 3D datasets and use the merged data to pretrain a universal 3D backbone. However, this solution overlooks the domain differences among different 3D point clouds, such as point densities, point signals, and noise characteristics. These differences can adversely affect pre-training quality and even reduce performance, as the work of PPT [43] observed. To address this issue, we conduct a comprehensive analysis of the domain discrepancy among 3D indoor scene datasets and identify key factors that may affect multi-source pretraining: varied data sparsity and varied signal variation across different datasets.

Based on our analysis on domain discrepancy, we present SWIN3D++, a novel architecture that extends the SWIN3D framework for multi-source pretraining, which tackles the domain discrepancy problem. Our main contributions are: (1) we design domain-specific mechanisms for SWIN3D, such as *domain-specific voxel prompts* that handle the sparse and uneven voxel distribution across domains and enhance the sparse-voxel feature attention in a multi-source setting, the *domain-modulated contextual relative signal embedding* scheme that captures the domain-specific signal variations and improves the contextual relative signal embedding using a tensor-decomposition-based representation, *domain-specific initial feature embedding* and *domain-specific layer normalization* that capture the data-source priors in a separate way; (2) we use a source-augmentation strategy that leverages different kinds of signals from the datasets to flexibly increase the amount of training data and boost the network pretraining.

We conducted supervised multi-source pretraining of SWIN3D++ on two indoor scene datasets with different data characteristics: Structured3D [55] and ScanNet [9]. We tested the performance and generalizability

*Interns at Microsoft Research Asia. †Contact person.

of SWIN3D++ on various downstream tasks, such as 3D semantic segmentation, 3D detection, and instance segmentation. The results demonstrate that SWIN3D++ outperforms the state-of-the-art methods and achieves: 78.2 mIoU on ScanNet segmentation (Val), 64.1 mAP @0.5 on ScanNet 3D detection, 80.2 mIoU on 6-fold S3DIS segmentation, and 60.7 mAP @0.5 on S3DIS 3D objection detection. We also performed comprehensive ablation studies to validate the effectiveness of our architectural design. Moreover, we demonstrated that fine-tuning the domain-specific parameters of SWIN3D++ is a powerful and efficient strategy for data-efficient learning, achieving a significant improvement over existing approaches.

2. Related Work

2.1. 3D Point Cloud Pretraining

In this section, we provide a brief overview of the recent developments in point cloud pretraining, focusing on three key aspects: *backbone architectures*, *pretraining schemes*, and *datasets*. We also review the existing literature on multi-source training.

Backbone architectures Sparse-voxel-convolution [37, 8, 12] are efficient in memory and computation, and have been widely used as the core component in many 3D pretraining works built upon U-Net [24] or HRNet [35] architectures. However, recent works have demonstrated that transformer architectures adapted to point clouds [13, 53, 42, 27] or sparse voxels [20] can enhance feature learning through attention on large receptive fields, and have been applied to 3D pretraining [49, 26, 48]. Our work is based on the architecture of SWIN3D [48], which employs an efficient self-attention mechanism on sparse voxels that reduces the memory complexity from quadratic to linear, and we improve this approach for effective multi-source pretraining.

Pretraining schemes Many existing 3D pretraining methods employ self-supervised learning strategies, which do not require labeled data. The early approaches [47, 40] use Autoencoder or Generative Adversarial Networks to learn latent representations of 3D data, via reconstructing data or data distribution. Later methods [45, 38, 15, 52] adopt contrastive learning, which encourage the similarity between positive pairs and the dissimilarity between negative pairs of 3D data. Transformer models, which are powered by masked signal modeling, such as BEiT [2] and masked autoencoder [14], have also been extended to 3D pretraining [22, 50, 49, 26, 44, 46]. Recently, supervised 3D

pretraining has benefited from the rapid advancement of synthetic data generation, for instance, SWIN3D [48], is pretrained on a large synthetic dataset [55] in a supervised manner, outperforms the previous pretraining methods by a large margin.

Datasets Most existing methods rely on ShapeNet [4] and ScanNet [9] for pretraining, but these datasets have limited diversity and size: ShapeNet contains only 57k CAD models from 55 common man-made categories, while ScanNet offers semantic segmentation annotations for about 1.5k indoor scenes. Other 3D datasets, such as ABC [18] (one million CAD models) and 3RScan [33] (1482 RGBD scans), are seldom used for pretraining. Swin3D [48] demonstrate that large-scale data is essential for the performance of the pretrained backbone and use Structured3D [55], a synthetic indoor scene dataset that is 10 times larger than ScanNet. Previous studies also indicate that (1) the backbone pretrained on CAD models suffers from a domain gap when applied to scene-level downstream tasks, as reported by Point-Contrast [45], and (2) the performance improvement from large pretraining data depends on the capability of backbone architecture, as shown by Swin3D [48].

Multi-source training Multi-source training data can enhance model performance, but it also poses several challenges. One challenge in supervised learning is to handle the inconsistent label taxonomies across different datasets. Previous works in computer vision have addressed this challenge by various methods, such as aligning data taxonomies and correcting incompatible annotations [21], unifying label spaces with pseudo labeling [54], or using dataset-specific training protocols, losses, and outputs while sharing a common architecture [56]. The work of PPT [43] proposes a *language-guided categorical alignment* method to align the label spaces of multiple datasets for 3D point cloud pretraining, which we adopt in our multi-source supervised pretraining. Another challenge is to deal with the domain discrepancy, where multiple datasets have different data characteristics. A common solution is to apply *domain-specific normalization* to the network architecture, such as using separate batch normalization and instance normalization layers for each domain [31, 5, 16]. PPT [43] applied domain-specific batch normalization to their convolution-based backbone for multi-source 3D pretraining. Our work introduces domain-specific 3D self-attention and other modules that effectively reduce the domain discrepancy.

Dataset	Data type	Capture device	Point signal	Scene type
ScanNet [9]	real data	Structure sensor	P+C+N	commercial and residential rooms
S3DIS [1]	real data	Matterport camera	P+C+N	buildings of educational and office use
Structured3D [55]	synthetic data	virtual scan	P+C+N	professional house design

Table 1. Domain characteristics of point clouds of common 3D indoor scene datasets. The table excludes the differences in data annotation. P, C, and N stand for point coordinate, color, and normal, respectively.

Datasets	$d_{\mathcal{H}}(\mathcal{S}, \mathcal{T})$
ScanNet & Structured3D	1.994
ScanNet & S3DIS	1.976

Table 2. \mathcal{H} -divergence metrics of two different datasets, including {Structured3D, ScanNet} and {ScanNet, S3DIS}.

3. Domain Discrepancy Analysis

Different factors, such as scene locations, capture devices, reconstruction algorithms, and annotation methods, influence the data characteristics of 3D indoor scene datasets. These characteristics include point density and noise pattern, color quality, scene types and diversity, and annotation level and precision. These variations result in a *domain discrepancy* (or *domain gap*) among different datasets. Table 1 compares some data characteristics of a few representative 3D indoor scene datasets. In this section, we propose to use the \mathcal{H} -divergence [3] tool to quantify the domain discrepancy among different datasets Section 3.1, and choose two important factors: window sparsity and signal variation to further analyze the source of domain discrepancy in Sections 3.2 and 3.3. These analyses guide our network design for multi-source pretraining.

3.1. Evaluation of domain discrepancy

\mathcal{H} -divergence is a measure of the difference between two datasets \mathcal{S} and \mathcal{T} . It is based on the idea that if there is a large divergence between \mathcal{S} and \mathcal{T} , then there should exist a classifier $h : \mathbf{x} \rightarrow \{0, 1\}$ that can accurately separate the samples from \mathcal{S} and \mathcal{T} . The classifier h belongs to a set of domain classifiers \mathcal{H} , where each classifier assigns the label 0 to the sample $\mathbf{x}_{\mathcal{S}}$ from \mathcal{S} , and 1 to the sample $\mathbf{x}_{\mathcal{T}}$ from \mathcal{T} . The formal definition of \mathcal{H} -divergence is:

$$d_{\mathcal{H}}(\mathcal{S}, \mathcal{T}) = 2 \left(1 - \min_{h \in \mathcal{H}} (\text{err}_{\mathcal{S}}(h(\mathbf{x})) + \text{err}_{\mathcal{T}}(h(\mathbf{x}))) \right), \quad (1)$$

where $\text{err}_{\mathcal{S}}$ and $\text{err}_{\mathcal{T}}$ are the prediction errors of the classifier h for a given \mathbf{x} sampled from \mathcal{S} and \mathcal{T} , respectively. The \mathcal{H} -divergence quantifies the domain discrepancy that can be captured by domain classifiers. It has a range from $[0, 2]$ (negative values are unlikely to happen), with 0 indicating that no classifier can distinguish between the two datasets, and 2 indicating that

there exists a perfect classifier that can separate them completely. A higher value of \mathcal{H} -divergence implies a larger degree of domain discrepancy.

We conducted an experiment to measure the \mathcal{H} -divergence of two 3D indoor scene datasets: Structured3D, a large synthetic dataset, and ScanNet, a real scanning dataset. We used two domain classifiers trained on the original training split of both datasets: one with a 3D Sparse CNN encoder structure [8] and another with a SWIN3D-S encoder architecture [48]. As the task is relatively simple, in both network architectures, we use a simple multi-resolution encoder to extract the global feature of each scene. In each resolution, we only use two Sparse CNN Resblocks or two SWIN3D blocks followed by a downsample layer. For each training batch, we ensured a balanced data distribution from the two datasets (1 : 1) and randomly cropped a 5m^3 cubic region from the input point cloud as the encoder input. To estimate the \mathcal{H} -divergence, we used a fixed set of cropped point cloud regions from the validation sets of both datasets and computed the prediction errors of the classifiers. As shown in Table 2, there is a significant domain discrepancy between Structured3D and ScanNet. We also measured the \mathcal{H} -divergence between ScanNet and S3DIS [1], which are both real-world datasets, and found that it is slightly lower than that between Structured3D and ScanNet. This indicates that the domain discrepancy between real-world datasets is also significant.

3.2. Window sparsity

Many 3D deep learning models for 3D point cloud learning adopt either 3D convolution or self-attention mechanisms to process local regions formed by sparse voxels. The number of occupied voxels in each region depends on both the point sampling method and the 3D content of the scene. To investigate how this number varies across different 3D indoor scene datasets, we conduct the following analysis.

We voxelize the point cloud of a 3D scene into a sparse grid with a uniform voxel size of 2 cm. We then partition the grid into non-overlapping windows of size $5 \times 5 \times 5$. For each non-empty window w , we calculate its *window occupancy ratio* w_{or} , which is the fraction of occupied voxels in w . The normalized cumulative

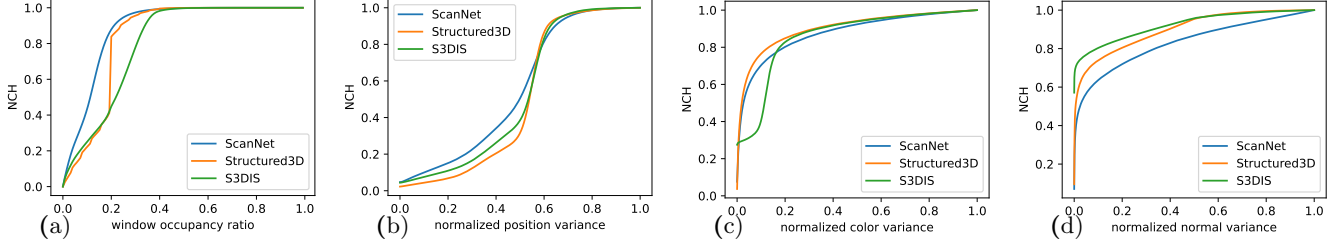


Figure 1. Window sparsity and signal variation analysis on windows of size $5 \times 5 \times 5$. The voxel size is set to 2 cm. (a) The normalized cumulative histogram (NCH) of the ratio of occupied voxels in the window. (b), (c), and (d) represent the NCHs of the variances of the positions, colors, and normals of the points in the window, respectively. All statistical calculations are based on the average of 200 scenes for each dataset. The variance ranges are normalized to $[0, 1]$ in the figures.

histogram (NCH) of w_{or} reveals the sparsity pattern of the scene at the window level. Fig. 1-(a) shows the averaged NCH for three datasets: ScanNet, Structure3D, and S3DIS. We can see that these datasets have different degrees of window sparsity. In particular, the NCH curve of Structured3D has a sharp increase at $w_{or} = \frac{1}{5}$. This is because Structured3D contains many clean vertical and horizontal planes that fill up 5×5 voxels within a $5 \times 5 \times 5$ window.

3.3. Signal variation

The input to the 3D neural networks often consists of the relative changes of point signals, such as position, color, and normal. To examine how these relative changes vary across different datasets, we propose the following evaluation strategy.

We adopt the same configuration as described in Section 3.2, and compute the variances of point position, color, and normals within a window w , denoted by Var_p , Var_c , and Var_n respectively: $\text{Var}_p = \frac{1}{2N^2} \sum_{x,y \in w} \|\mathbf{p}(x) - \mathbf{p}(y)\|^2$; $\text{Var}_c = \frac{1}{2N^2} \sum_{x,y \in w} \|\mathbf{c}(x) - \mathbf{c}(y)\|^2$; $\text{Var}_n = \frac{1}{2N^2} \sum_{x,y \in w} \|\mathbf{n}(x) - \mathbf{n}(y)\|^2$. Here, \mathbf{p} , \mathbf{c} , and \mathbf{n} represent point coordinate, color, and normal respectively, while N is the number of non-empty voxels in w . Following existing 3D learning approaches, we resample the input point cloud to ensure that each non-empty voxel contains only one point. To assess the distribution of signal variance, we use the normalized cumulative histogram (NCH). Fig. 1-(b,c,d) show the averaged NCH for three datasets (ScanNet, Structure3D, and S3DIS) with respect to Var_p , Var_c , and Var_n respectively. The position variance NCH curve of Structured3D indicates that it has more diverse geometric changes in shape than the other two datasets. Moreover, the color variance NCH curve of Structured3D reveals that its synthetic color richness is still lower than the other two real datasets. Lastly, the lower NCH curve of normal variance for ScanNet suggests that its normal data is noisier than the other datasets.

4. Methodology

In this section, we first provide a concise overview of the SWIN3D network architecture[48] (Section 4.1) and then introduce our novel modifications to SWIN3D that enable effective multi-source pretraining (Section 4.2).

4.1. Recap of SWIN3D

SWIN3D is a novel 3D backbone architecture for point cloud analysis that adopts the Swin Transformer[23] model. It uses a hierarchical network structure that converts the input point cloud into a multi-scale sparse voxel grid. The initial feature embedding layer transforms the raw voxel features into a high-dimensional space using sparse convolution. Then, the voxel features are processed by a sequence of SWIN3D blocks and down-sampled at different scales. Each SWIN3D block applies memory-efficient self-attention to the sparse voxel features within regular or shifted windows. To enhance the feature learning capability, its self-attention mechanism employs *contextual relative signal encoding* (cRSE), which utilizes learnable look-up tables to map the relative signal changes to high-dimensional features and integrates these content-aware features into the self-attention computation. Fig. 2-(a) shows the SWIN3D network architecture. We briefly review the key components of SWIN3D below.

Input The input point cloud \mathcal{S} consists of points with feature vectors $\mathbf{s}_p \in \mathbb{R}^M$, which include point coordinates and other signal information such as point color and normal if available.

Voxelization \mathcal{S} is voxelized into a sparse voxel grid with five levels of resolution, where the finest voxel size is 2 cm for indoor scenes. For each nonempty voxel, a *representative point* is chosen from the points within the voxel, and the voxel feature is set as the feature of its *representative point*.

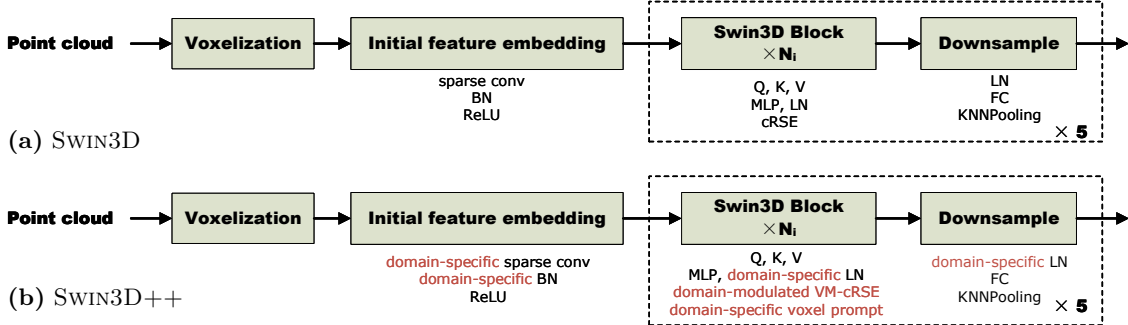


Figure 2. Overview of network architectures of SWIN3D and SWIN3D++. $N_1, N_2, N_3, N_4, N_5 = 2, 4, 9, 4, 4$. BN, LN and FC refer to *batch normalization*, *layer normalization* and *fully-connected layer*. Q, K, V are Key, Query and Value tensors of self-attention.

Initial feature embedding A sparse convolution layer with kernel size 3 is applied to the voxels at the finest level, followed by a BatchNorm (BN) layer and a ReLU layer. The voxel feature that is used for the convolution is the concatenation of the positional offset to the voxel center and other point signals.

Swin3D block The SWIN3D block performs self-attention on regular and shifted windows in 3D, with window size $M \times M \times M$. It adopts the standard transformer architecture, consisting of multi-head self-attention, LayerNorm layers (LN) and an MLP layer. It enhances its self-attention with a memory-efficient implementation and a contextual relative signal encoding scheme (cRSE), and the computation formula is given as follows (we omit the multi-head notation for simplicity).

Let $\{\mathbf{f}_i\}_{i=1}^N$ denote the feature vectors of nonempty voxels $\{\mathbf{v}_i\}_{i=1}^N$ in a given window. Linear projection tensors $\mathbf{W}_Q, \mathbf{W}_K, \mathbf{W}_V$ are defined for *Query*, *Key*, and *Value*, respectively. The self-attention mechanism computes the output feature vector \mathbf{f}_i^* at each voxel \mathbf{v}_i as follows:

$$\mathbf{f}_i^* = \frac{\sum_{j=1}^N \exp(e_{ij})(\mathbf{f}_j \mathbf{W}_V + \mathbf{t}_V(\Delta \mathbf{s}_{ij}))}{\sum_{j=1}^N \exp(e_{ij})}, \quad (2)$$

where e_{ij} is the scaled attention score between the query vector $\mathbf{f}_i \mathbf{W}_Q$ and the key vector $\mathbf{f}_j \mathbf{W}_K$, given by:

$$e_{ij} = \frac{(\mathbf{f}_i \mathbf{W}_Q)(\mathbf{f}_j \mathbf{W}_K)^T + b_{ij}}{\sqrt{d}}, \quad (3)$$

with d being the channel dimension. The term b_{ij} is the contextual relative signal encoding of the displacement vector $\Delta \mathbf{s}_{ij} := \mathbf{s}_{\mathbf{v}_i} - \mathbf{s}_{\mathbf{v}_j}$, which captures the contextual relation between the query and the key voxels. It is computed as:

$$b_{ij} = (\mathbf{f}_i \mathbf{W}_Q)(\mathbf{t}_K(\Delta \mathbf{s}_{ij}))^T + (\mathbf{f}_j \mathbf{W}_K)(\mathbf{t}_Q(\Delta \mathbf{s}_{ij}))^T. \quad (4)$$

Net	single-source	multi-source
SWIN3D	76.8	76.5
SparseUNet	75.8	73.6

Table 3. Naive multi-source pretraining does not lead better performance on ScanNet segmentation (validation set). The results of SparseUNet are from Tab. 2(a) & Tab. 3 of [43]. The reported values are mean IoUs of segmentation.

Here, $\mathbf{t}_V, \mathbf{t}_K, \mathbf{t}_Q$ are trainable functions that map the bounded $\Delta \mathbf{s}_{ij}$ to \mathbb{R}^d . These functions are implemented as look-up tables, following the approach of [20, 41].

Downsample The Downsample module of SWIN3D performs two steps. First, it applies a LayerNorm layer and a fully connected (FC) layer to each voxel feature vector. Second, it uses KNNpooling to aggregate the features of the nearest neighbors for the downsampled voxels.

Limitations of naive multi-source pretraining Pretraining SWIN3D on multiple datasets by combining data alone does not guarantee better performance on downstream tasks. This is evident from the results of SWIN3D pretrained on Structured3D only and SWIN3D pretrained on both ScanNet and Structured3D. The former outperforms the latter on the downstream task of ScanNet semantic segmentation, as shown in Table 3. This finding is consistent with [43], which also observed lower performance of SparseUNet pretrained on three datasets: ScanNet, Structured3D and S3DIS, without considering domain discrepancy.

4.2. Design of SWIN3D++

To address the aforementioned issues in multi-source pretraining, we introduce SWIN3D++, a novel approach that enhances the SWIN3D model with several domain-specific components. These components are

designed to isolate the domain-specific features from the shared backbone, resulting in better performance and generalization across different domains. The components include: *domain-specific initial feature embedding* (Section 4.2.3), *domain-specific layer normalization* (Section 4.2.2), *domain-specific voxel prompts* (Section 4.2.3), *domain-modulated cRSE* (Section 4.2.4) and its enhanced version — *domain-modulated VM-cRSE* (Section 4.2.5), and a *source augmentation* strategy (Section 4.2.6). We illustrate the main differences between our approach and the original SWIN3D architecture in Fig. 2-(b).

We use the notation $\{\mathcal{D}_l\}_{l=1}^L$ to denote the multiple datasets that we use for pretraining, where L is the number of datasets. We allow different input signal types for different datasets. For instance, the point clouds in \mathcal{D}_1 may only have point coordinates, while the point clouds in \mathcal{D}_2 may have both point coordinates and color information.

4.2.1 Domain-specific initial feature embedding

We use a separate feature embedding module for each data source to obtain the initial embeddings of the raw point features. This allows the module to capture the data-source priors and properties during the pretraining process. We refer to this module as *domain-specific*, meaning that the network contains L different feature embedding modules during the pretraining. This design slightly increases the network parameters, as the feature embedding module is lightweight.

4.2.2 Domain-specific layer normalization

To take domain discrepancy into account, we introduce domain-specific layer normalization (DSLN) for SWIN3D, inspired by the concept of domain-specific batch normalization and instance normalization [31]. DSLN allows each data source to have its own element-wise affine transformation in the LN layer, instead of sharing the same parameters. The DSLN formula for data $\mathcal{S} \in \mathcal{D}_l$ is given by:

$$\mathbf{f}^* = \frac{\mathbf{f} - \mathbb{E}[\mathbf{f}]}{\sqrt{\text{Var}[\mathbf{f}] + \epsilon}} \cdot \gamma_l + \beta_l, \quad (5)$$

where $\mathbb{E}[\mathbf{f}]$ and $\text{Var}[\mathbf{f}]$ are the mean and variance of all voxel features, computed over channel dimension. The parameters of γ_l and β_l are domain-specific parameters, and ϵ is a small constant to prevent numerical instability. This modification is simple but effective, and has not been explored by previous work for both multi-source training and pretraining.

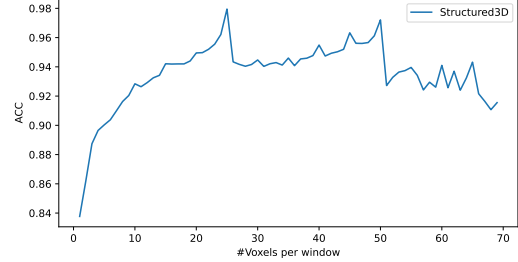


Figure 3. Segmentation accuracy of SWIN3D on the Structured3D validation set. The x-axis represents the count of nonempty voxels in a $5 \times 5 \times 5$ grid with a voxel size of 2 cm. The y-axis indicates the average segmentation accuracy across windows with an equal number of nonempty voxels.

4.2.3 Domain-specific voxel prompts

Since SWIN3D calculates self-attention between nonempty voxels within a window, we hypothesize that windows with very few voxels have limited information exchange, and the learned voxel features in such windows may be less effective. To validate this hypothesis, we evaluate the segmentation accuracy of SWIN3D on the Structured3D dataset. We compute the average voxel accuracy for windows with the same number of nonempty voxels and visualize the accuracy curve in Fig. 3. The findings clearly demonstrate that windows containing less than 10 nonempty voxels exhibit considerably lower accuracy in comparison to others.

We address the above issue across different datasets by introducing a set of virtual voxels $\{\tilde{\mathbf{v}}_b\}_{b=1}^B$ into each SWIN3D block, which are referred to as *domain-specific voxel prompts*. These virtual voxels are not shared by different SWIN3D blocks, and each virtual voxel $\tilde{\mathbf{v}}_b$ is associated with a learnable and domain-specific feature vector $\{\tilde{\mathbf{f}}_b\}$. This helps to reduce the extreme window sparsity issue and provides data-source prior to guide the feature learning. The self-attention formula is revised to take into account these additional voxels and features:

$$\mathbf{f}_i^* = \left(\sum_{j=1}^N \exp(e_{ij})(\mathbf{f}_j \mathbf{W}_V + \mathbf{t}_V(\Delta \mathbf{s}_{ij})) + \sum_{b=1}^B \exp(\tilde{e}_{ib})(\tilde{\mathbf{f}}_b \mathbf{W}_V) \right) / \left(\sum_{j=1}^N \exp(e_{ij}) + \sum_{b=1}^B \exp(\tilde{e}_{ib}) \right), \quad i = 1, \dots, N, \quad (6)$$

where e_{ij} is the same to Eq. (3) and

$$\tilde{e}_{ib} = \frac{(\mathbf{f}_i \mathbf{W}_Q)(\tilde{\mathbf{f}}_b \mathbf{W}_K)^T}{\sqrt{d}}, \quad b = 1, \dots, B \quad (7)$$

Here note that there is no contextual relative signal encoding between virtual voxels and real voxels in the above formulae as the virtual voxels are not bind with any raw features. In our implementation, we empirically choose $B = 5$ to strike a balance between performance and efficiency.

4.2.4 Domain-Modulated cRSE

To encode the raw signal differences that vary across different datasets, as demonstrated in Section 3.3, the cRSE in SWIN3D needs to be adapted for each dataset during pretraining. A straightforward solution is to use a *domain-specific* cRSE, but this would increase the parameter size of SWIN3D rapidly, making it difficult to fit the network of SWIN3D in GPUs with limited memory when pretraining with multiple datasets. Therefore, we propose an alternative solution, called *domain-modulated cRSE*, which leverages a shared base cRSE for multiple datasets and applies a domain-specific modulation to the base cRSE.

Base cRSE The base cRSE is identical to the original cRSE, and we use the same symbols $\mathbf{t}_V, \mathbf{t}_K, \mathbf{t}_Q$ to represent them. We express the signal difference $\Delta \mathbf{s}$ between voxel \mathbf{u} and \mathbf{v} as a vector: $(\delta_1, \dots, \delta_m)$, corresponding to the three components of coordinate, color, and normal, respectively. We write the base cRSE as follows:

$$\mathbf{t}_R(\Delta \mathbf{s}) = \sum_{m=1}^M \mathbf{t}_m(\delta_m^q), \quad R \in \{Q, K, V\} \quad (8)$$

where δ_m^q is a quantized version of δ_m and \mathbf{t}_m is a trainable look-up table that maps δ_m^q to the feature space.

Domain modulation In each SWIN3D block, we introduce a set of domain-specific look-up tables $\{\mathbf{t}_m^l, l = 1, \dots, L\}$ to modulate the base cRSE.

$$\mathbf{t}_{R,l}(\Delta \mathbf{s}) = \sum_{m=1}^M \mathbf{t}_m^l(\delta_m^q) \cdot \mathbf{t}_m(\delta_m^q), \quad R \in \{Q, K, V\} \quad (9)$$

where \mathbf{t}_m^l maps δ_m^q to a scalar value. To apply the domain-aware cRSE formulation, we only need to substitute $\mathbf{t}_V, \mathbf{t}_K, \mathbf{t}_Q$ in Eq. (6) with $\mathbf{t}_{V,l}, \mathbf{t}_{K,l}, \mathbf{t}_{Q,l}$. The additional parameters introduced by all \mathbf{t}_m^l s per SWIN3D block are tiny, as they amount only to $3 \times M \times L \times T$, where T is the number of quantization divisions and 3 refers to $\{Q, K, V\}$. When cRSE uses point coordinate, color and normal, M is equal to 9.

4.2.5 Domain-Modulated VM-cRSE

To encode relative signal changes optimally, one should account for the correlation of the changes in all dimensions. A possible implementation is to use a look-up table with a T^M grid for mapping the quantized changes. This approach is called the *Product method* in the previous work[41]. However, this method suffers from high storage cost when M is large and low utilization rate of the grid table, as the signal changes are sparse in \mathbb{R}^M space. A simpler approximation of this method is the *cross method* in [41], which is given by Eq. (8), but it has a limited ability to capture correlation among different signal dimensions.

VM-cRSE We take a different view at the T^M grid table mentioned above: the grid can be regarded as a Tensor with dimension $T \times T \times \dots \times T \times C$, where C is the feature dimension. Without loss of generality, we assume $M = 9$ which represents the changes of point coordinates, colors and normals. Inspired by Vector-Matrix (VM) decomposition [6], we propose to approximate the grid table by VM in the following way, with the balance between efficiency and capability.

We first disregard the correlation between different types of signals, for instance, the red color channel and the x-direction of the normal, as they have no deep correlation in general. Thus, the large grid table can be replaced by three different T^3 grid tables: $\mathcal{T}_p, \mathcal{T}_c, \mathcal{T}_n$. We utilize VM decomposition to approximate them:

$$\begin{aligned} \mathcal{T}_r(\delta_r^q) = & \mathbf{t}_{r,1}(\delta_{r,1}^q) \cdot \mathbf{t}_{r,23}(\delta_{r,2}^q, \delta_{r,3}^q) + \\ & \mathbf{t}_{r,2}(\delta_{r,2}^q) \cdot \mathbf{t}_{r,31}(\delta_{r,3}^q, \delta_{r,1}^q) + \\ & \mathbf{t}_{r,3}(\delta_{r,3}^q) \cdot \mathbf{t}_{r,12}(\delta_{r,1}^q, \delta_{r,2}^q), \quad r \in \{p, c, n\}. \end{aligned} \quad (10)$$

Here, $\{1, 2, 3\}$ in the subscripts denote the first, second and third component of the corresponding signal; $\mathbf{t}_{r,k}$ and $\mathbf{t}_{r,kj}$ are 1D and 2D look-up tables that maps the relative 1D and 2D changes to the feature space.

With the above VM decomposition, Eq. (8) can be replaced by:

$$\mathbf{t}_R(\Delta \mathbf{s}) = \sum_{r \in \{p, c, n\}} \mathcal{T}_r(\delta_r^q), \quad R \in \{Q, K, V\}. \quad (11)$$

We call the above formulation — *VM-cRSE*.

Domain-modulated VM-cRSE To enable multi-source pretraining, we extend the method described in Section 4.2.4 to incorporate *domain-awareness* into the VM-cRSE: we use a collection of domain-specific 1D and 2D look-up tables $\{\mathbf{t}_{r,k}^l, l = 1, \dots, L\}$ and $\{\mathbf{t}_{r,kj}^l, l = 1, \dots, L\}$ to adjust the base cRSEs. The equation in

Eq. (10) is modified as follows:

$$\begin{aligned} \mathcal{T}_r^l(\delta_r^q) &= \mathbf{t}_{r,1}^l(\delta_{r,1}^q) \cdot \mathbf{t}_{r,1}^l(\delta_{r,1}^q) \cdot \mathbf{t}_{r,23}^l(\delta_{r,2}^q, \delta_{r,3}^q) \cdot \mathbf{t}_{r,23}^l(\delta_{r,2}^q, \delta_{r,3}^q) \\ &+ \mathbf{t}_{r,2}^l(\delta_{r,2}^q) \cdot \mathbf{t}_{r,2}^l(\delta_{r,2}^q) \cdot \mathbf{t}_{r,31}^l(\delta_{r,3}^q, \delta_{r,1}^q) \cdot \mathbf{t}_{r,31}^l(\delta_{r,3}^q, \delta_{r,1}^q) \\ &+ \mathbf{t}_{r,3}^l(\delta_{r,3}^q) \cdot \mathbf{t}_{r,3}^l(\delta_{r,3}^q) \cdot \mathbf{t}_{r,12}^l(\delta_{r,1}^q, \delta_{r,2}^q) \cdot \mathbf{t}_{r,12}^l(\delta_{r,1}^q, \delta_{r,2}^q), \\ r &\in \{p, c, n\}. \end{aligned} \tag{12}$$

$\mathbf{t}_{r,k}^l$ and $\mathbf{t}_{r,kj}^l$ map the quantized signal changes (1D or 2D) to scalar values. Domain-modulated VM-cRSE is by default used in SWIN3D++. During the training phase, the shared look-up tables are initialized by a Gaussian distribution whose mean is 0 and variance is 0.02, and all look-up tables for domain modulation are initialized to 1.

4.2.6 Source augmentation

To analyze point clouds, we often need to consider different types of signals associated with the points, such as coordinates, color, normal, and voxel occupancy. However, most existing methods use a fixed set of signals as input to the network, which limits their generalization ability to handle data with varying signal types. For example, if the input data have more or fewer signals than expected, one may have to discard or fabricate some signals, and retrain or finetune the network accordingly.

On the other hand, our multi-source pretraining setting allows us to leverage the different types of signals from multiple point clouds to enhance the pretraining performance. We introduce a source-augmentation strategy to expand the pretraining datasets, as follows. Without loss of generality, we assume that a dataset \mathcal{A} consists of three types of signals: point coordinates (p), color (c), and normal (n). We can create multiple datasets from \mathcal{A} with various combinations of signals: $\mathcal{A}_p, \mathcal{A}_{pc}, \mathcal{A}_{pn}, \mathcal{A}_{pcn}$. By mixing these augmented datasets with other datasets, we can increase the quantity and diversity of data for pretraining without extra cost. The enlarged datasets are beneficial to pretrain the shared parameters of the networks, and signal-specific data features can be learned by our domain-specific network design.

Adaption for domain-modulated cRSE In order to facilitate domain-modulated cRSE for augmented sources with different signal types, we introduce virtual point signal types that may not be present in certain augmented datasets. These virtual point signal types are used solely for cRSE computation, and we assume that the added point signal values are identical. This ensures that the relative signal changes are always zero, allowing the domain-modulated look-up tables to only map the zero change to a learnable scalar value.

5. Experimental Analysis

In this section, we first present the detailed configuration of the multi-source pretraining of SWIN3D++ (Section 5.1), and demonstrate the effectiveness of the proposed modules through comprehensive ablation studies (Section 5.2). In Section 5.3, we report the performance of the finetuned SWIN3D++ on typical downstream tasks on indoor scenes, and demonstrate its advantage over existing methods in both fully-annotated and weakly-annotated settings.

5.1. Multi-source pretraining

Network configuration Swin3D [48] proposed two versions of pretrained models: SWIN3D-S and SWIN3D-L. Both versions have the same configuration of window sizes and block layers: the first stage has a window size of $5 \times 5 \times 5$ and the rest have $7 \times 7 \times 7$, and the layer numbers are $\{2, 4, 9, 4, 4\}$. However, SWIN3D-L has more feature channels and attention heads than SWIN3D-S, which improves its performance but also increases its data and resource requirements. We designed SWIN3D++ based on the structure of SWIN3D-S, aiming to balance performance and pretraining cost on multiple datasets. We set the quantization division numbers to 16 for 1D look-up tables and 4×4 for 2D look-up tables, respectively. Table 4 compares the parameter sizes of SWIN3D-S, SWIN3D-L and SWIN3D++, where the shared parameters of SWIN3D blocks of SWIN3D++ is larger than SWIN3D-S due to the use of 2D tables.

Pretraining setting We use Structured3D [55] (21 K synthetic rooms) and ScanNet [9] (1.5 K scanned rooms) as our pretraining datasets, and choose 3D semantic segmentation as the pretext task. We generate point clouds from Structured3D following [48], with color, normal, and semantic label information for each point. However, the semantic labels of Structured3D and ScanNet are not compatible, so we cannot use them directly for supervised learning. To solve this problem, we apply *language-guided categorical alignment* [43], which leverages the relationship between label texts to unify the label space. We use the same decoder architecture as in the pretraining of SWIN3D [48] to predict the semantic labels. The only modification is that we replace the LayerNorm in decoder with a *domain-specific* one to handle multi-source inputs.

Training details We follow the original data split of Structured3D and ScanNet. To balance the two datasets, we use a ratio of 2 : 1, meaning that for every three batches, two contain only Structured3D data and one contains only ScanNet data. We augment the input

Net	FE.(M)	blocks (M)	Other (M)	Total (M)
SWIN3D-S	0.01	22.87	0.69	23.57
SWIN3D-L	0.01	58.82	0.69	60.75
SWIN3D++	$L \times 0.01$	$L \times 1.79 + 46.22$	$L \times 0.01 + 0.69$	$L \times 1.81 + 46.91$

Table 4. Net parameters of individual modules. L represents the number of datasets. **FE**, **blocks**, **Other** refer to *initial feature embedding*, *SWIN3D blocks*, and *all the remaining modules*, respectively.

data by randomly cropping and rotating them. We train the network for 100 epochs on 8 NVIDIA V100 GPUs (32 GB), using the AdamW optimizer with a Cosine learning rate scheduler, and taking 6 days.

Network efficiency The network inference stage is efficient in terms of GPU memory and time. It requires only 6 GB of GPU memory on average, and it completes the inference in 900 ms for each scene, on average.

5.2. Ablation study

We conduct an ablation study to examine the effectiveness of the proposed modules of SWIN3D++ for multi-source pretraining. We compare different pre-training settings of SWIN3D++ as follows:

- (1) Baseline. We use the SWIN3D-S network structure and pretrain it only on Structured3D data.
- (2) Baseline + Multi-source. We pretrain SWIN3D-S on both Structured3D and ScanNet with *language-guided categorical alignment* [43].
- (3) Based on (2), we introduce *domain-specific initial feature embedding*.
- (4) Based on (3), we apply *domain-specific layer normalization*.
- (5) Based on (4), we replace the shared cRSE with *domain-modulated cRSE*.
- (6) Based on (5), we replace *domain-modulated cRSE* with *domain-modulated VM-cRSE*.
- (7) Based on (6), we add *domain-specific voxel prompt*.
- (8) Based on (7), we enable *source augmentation*. This is our default setting of SWIN3D++.

We test our pretraining setting on the 3D semantic segmentation task, using ScanNet (validation set) and S3DIS (Area 5) as the benchmarks. We measure the performance by the mean IoU metric. It is important to note that the S3DIS dataset was not used for the pretraining, so the performance on this dataset reflects the generalization ability of the pretrained backbones. We follow the setup of SWIN3D on the 3D segmentation task, which adds a SWIN3D block at each level of the

ID	Pretraining settings						Segmentation mIoU(%)	
	MS	DI	DL	DM-cRSE	VP	SA	ScanNet	S3DIS
(1)	✗	✗	✗	✗	✗	✗	76.8	72.5
(2)	✓	✗	✗	✗	✗	✗	77.0	72.8
(3)	✓	✓	✗	✗	✗	✗	77.0	73.0
(4)	✓	✓	✓	✗	✗	✗	77.2	73.2
(5)	✓	✓	✓	DM	✗	✗	77.3	73.2
(6)	✓	✓	✓	VM	✗	✗	77.6	73.4
(7)	✓	✓	✓	VM	✓	✗	77.8	74.0
(8)	✓	✓	✓	VM	✓	✓	78.2	74.9
(9)	✓	✓	✗	VM	✓	✓	77.6	73.9

Table 5. Ablation study of SWIN3D++ modules. **MS**, **DI**, **DL**, **DM-cRSE**, **VP**, **SA** refer to using multi-source datasets, domain-specific initial feature embedding, domain-specific LayerNorm, domain-modulated cRSE (DM) or domain-modulated VM-cRSE (VM), domain-specific voxel prompt and source augmentation.

decoder after the skip-connection. We also activate the domain-specific modules in the decoder if they are activated in the corresponding SWIN3D++ encoder in the ablation study. The input signals of points in the benchmark include point coordinate, normal and color. For finetuning, we load the shared parameters and the domain-specific module parameters corresponding to the ScanNet dataset if they exist. We finetune the models for 600 epochs on ScanNet and 3000 epochs on S3DIS.

The results reported in Table 5 show that the performance increases gradually as we adopt more components from our default setting. In particular, we found that: *domain-modulated VM-cRSE* contributes significantly to the performance on ScanNet; *source augmentation* and *domain-specific voxel prompt* lead to the most noticeable improvement on S3DIS. We also observe that *domain-specific layer normalization* plays a crucial role in boosting the performance of other modules: when we use a shared LayerNorm across different sources, the results deteriorate significantly, as shown in Table 5-(9), compared to (8). We notice that the improvement achieved by *domain-modulated cRSE* is marginal (see (4)&(5)), because it has few trainable parameters. However, its improved variant *domain-modulated VM-cRSE* is more effective (see (4)&(6)), as it has more parameters that are derived from 2D look-up tables.

To assess the impact of the *domain-specific voxel prompt* on prediction accuracy, especially on windows with less nonempty voxels, we conduct a similar evalua-

Method	Pre.	ScanNet Segmentation		S3DIS Segmentation	
		Val mIoU (%)	Test mIoU (%)	Area5 mIoU (%)	6-fold mIoU (%)
LargeKernel3D [7]	✗	73.5	73.9	-	-
Mix3D [25]	✗	73.6	78.1	-	-
Stratified Transformer [20]	✗	74.3	74.7	72.0	-
PointTransformerV2 [42]	✗	75.4	75.2	71.6	-
OctFormer [36]	✗	75.7	76.6	-	-
PointVector-XL [10]	✗	-	-	72.3	78.4
WindowNorm [39]	✗	-	-	72.2	77.6
OneFormer3D [19]	✗	76.6	-	-	-
DepthContrast [51]	ScanNet	71.2	-	70.6	-
SceneContext [15]	ScanNet	73.8	-	72.2	-
PointContrast [45]	ScanNet	74.1	-	70.9	-
MaskContrast [44]	ScanNet	75.5	-	-	-
SWIN3D-S [48]	Structured3D	76.8	-	73.0	78.2
SWIN3D-L [48]	Structured3D	77.5	77.9	74.5	79.8
OneFormer3D [19]	ScanNet+Structured3D	-	-	72.4	75.0
PPT [43]	ScanNet+Structured3D+S3DIS	76.4	76.6	72.7	78.1
PonderV2 [57]	ScanNet+Structured3D+S3DIS	77.0	78.5	73.2	79.1
SWIN3D++	ScanNet+Structured3D	78.2	77.7	74.9	80.2

Table 6. Quantitative evaluation on semantic segmentation. **Pre.** indicates whether the method uses pretraining and which datasets are used. DepthContrast, SceneContext, PointContrast and MaskContrast are pretrained in a self-supervised manner, and other pretraining-based methods utilize data labels. The hyphen symbol (-) denotes that the method does not perform a certain task. We report the best scores achieved by different methods.

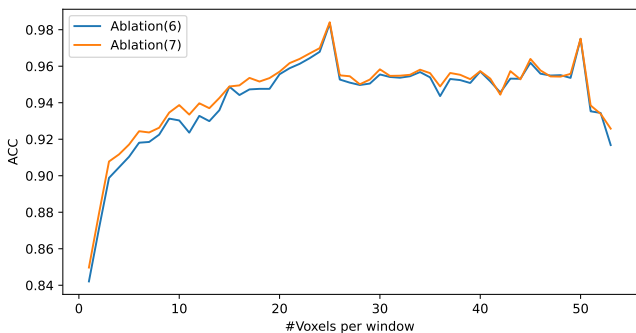


Figure 4. Effect of *domain-specific voxel prompt* on the segmentation accuracy on the Structure3D validation set.

tion as in Fig. 3 on the pretrained SWIN3D++ model with the ablation settings (6) and (7). Figure 4 shows that the accuracy on windows with fewer nonempty voxels is improved clearly by introducing the domain-specific voxel prompt, while the improvement on grids with more nonempty voxels is less noticeable, as there are enough nonempty voxels for feature interaction.

5.3. Evaluation on downstream tasks

We present the results of applying the multi-source pretrained SWIN3D++ to three common indoor scene understanding tasks: 3D semantic segmentation, 3D detection, and instance segmentation. We also test the data efficiency of our method. Similar to our ablation study, for all experiments, we use the same SWIN3D++ backbone that is pretrained on multiple sources and its domain-specific module parameters corresponding to the ScanNet dataset. We provide the details of our training setup and the performance of our approach in the following paragraphs.

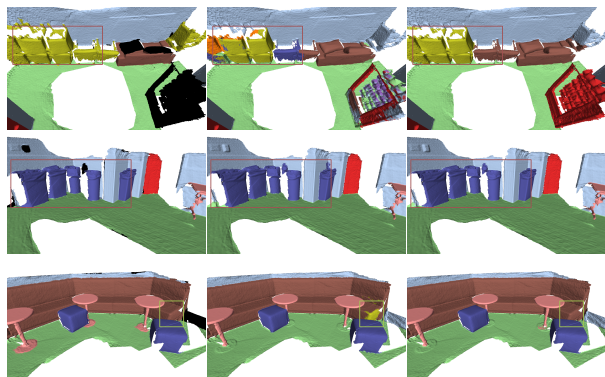


Figure 5. Visual comparison of ScanNet segmentation. **Left:** Ground-truth segmentation labels. **Middle:** SWIN3D-L [48]’s results. **Right:** SWIN3D++’s results.

3D semantic segmentation We conduct semantic segmentation on two widely used datasets: ScanNet and S3DIS. The data splits of ScanNet are 1201 (training), 312 (validation), 100 (test); and S3DIS contains 272 scenes across 6 areas. We adopt the same decoder and finetuning configurations as in our ablation study. We show the results on the ScanNet validation set, the ScanNet test set, Area 5 of S3DIS, and the S3DIS 6-fold cross-validation in Table 6. We also benchmark our method against existing approaches that use different training settings: training from scratch, pretrained with a single dataset, pretrained with multiple datasets. As shown in Table 6, the recent pretraining-based approaches, such as SWIN3D-S, SWIN3D-L, Point Prompt Training (PPT) [43], and PonderV2 [57] which used PPT for pretraining with a reconstruction-based pretext task, outperform most unprtrained methods on both tasks. Among them, our SWIN3D++ achieves the best

Method	Pre.	mAP@0.25	mAP@0.5
CAGroup3D [34]	✗	75.1	61.3
+ SWIN3D-L [48]	✓	76.4	63.2
+ SWIN3D++	✓	76.2	64.1
V-DETR [32]	✗	77.8	66.0

Table 7. Quantitative evaluation on 3D detection (ScanNet).

Method	Pre.	mAP@0.25	mAP@0.5
FCAF3D [29]	✗	66.7	45.9
+ SWIN3D-L [48]	✓	72.1	54.0
+ SWIN3D++	✓	75.5	60.7
Point-GCC+TR3D [11]	✓	75.1	56.7

Table 8. Quantitative evaluation of 3D detection (S3DIS).

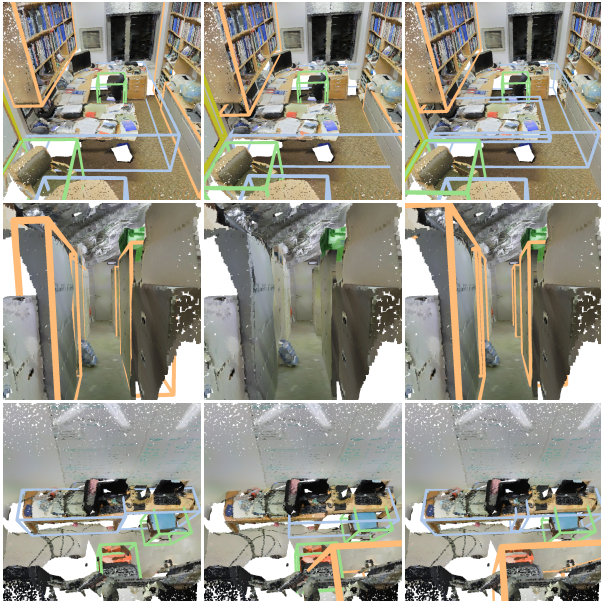


Figure 6. Visual comparison of 3D Detection on S3DIS scenes. **Left:** Ground-truth object boxes. **Middle:** FCAF3D+SWIN3D [48]’s results. **Right:** FCAF3D+SWIN3D++’s results.

performance on ScanNet(val) and S3DIS, but behind SWIN3D-L, Mix3D and PonderV2 on ScanNet(test). In Fig. 5, we provide visual comparison of SWIN3D-L and SWIN3D++ on three ScanNet(val) scenes, and highlight the improvement of SWIN3D++ over SWIN3D-L.

3D detection We adopt the same training setup and evaluation protocol as SWIN3D [48] to test the performance of SWIN3D++ on 3D detection. We use either CAGroup3D [34] or FCAF3D [29] as the detector architecture, and replace their original feature extractor with our pretrained SWIN3D++. Table 7 and Table 8 show the detection performance on ScanNet and S3DIS datasets, where we use mAP@0.25 and mAP@0.5 metrics to evaluate the results. We observe that the use of

pretrained SWIN3D++ achieves comparable mAP@0.25 score to SWIN3D, and significantly higher score on mAP@0.5. Notably, SWIN3D+++FCAF3D achieves the state-of-the-art performance on S3DIS. Fig. 6 visualizes the improvement of SWIN3D++ over SWIN3D-L on three S3DIS scenes. This demonstrates that multi-source pretraining via SWIN3D++ enhances 3D detection. We also note that the detectors we employed are not the best ones, and more advanced architectures such as V-DETR [32] can achieve state-of-the-art performance. It is promising to combine our backbone with the latest detector design to further improve the performance.

3D instance segmentation We follow the experimental setup of MaskContrast [44] and PPT [43] to evaluate our approach on 3D instance segmentation, where PointGroup [17] is the baseline method for the instance segmentation task. The original design of PointGroup uses Sparse-conv-based UNet as the backbone, which we replace with our pretrained SWIN3D++. We also compare our backbone with the pretrained SWIN3D-S. We select ScanNet and ScanNet200 datasets as testbeds, where the latter dataset is a fine-grained ScanNet dataset with 200 object categories. Table 9 shows the common metrics (mAP, mAP@0.50, mAP@0.25) of different approaches. We observe that multi-source training (PPT and SWIN3D++) significantly improves the performance over the baseline, while SWIN3D++ is the best one among the approaches that use PointGroup architecture. However, more optimal instance segmentation designs like Mask3D outperform PointGroup, so there is an opportunity to integrate them with our pretrained backbone.

Data efficient learning We use the ScanNet200 segmentation task [28] for data efficient learning. ScanNet200 has 200 class categories, far more than 20 categories of the original ScanNet; and the labels have not been leaked to the pretraining. We follow the data-efficient split from SceneContext [15] to finetune the backbone and report the mean mIoU on the validation set, in which 1%, 5%, 10%, 20% data are chosen as training data. Note that the 1% split only has 12 scenes for training. To avoid overfitting the limited data, we use a simple segmentation decoder like in the pretraining stage. We compare SWIN3D++ with other pretrained models, such as SWIN3D [48] and PPT [43]. The results show that SWIN3D++ achieves significant improvements over other methods, including PPT [43], which is supervisedly pretrained on three datasets. Moreover, we find that finetuning only the domain-specific modules is a parameter-efficient way to adapt to the limited

Method	Pre.	ScanNet			ScanNet200		
		mAP	mAP@0.50	mAP@0.25	mAP	mAP@0.50	mAP@0.25
Mask3D [30]	\times	55.2	78.0	87.0	-	-	-
PointGroup [17]	\times	36.0	56.9	72.8	15.8	24.5	32.2
+ MaskContrast [44]	ScanNet	-	59.6	-	-	26.8	-
+ SWIN3D-S [48]	Structured3D	39.2	61.5	76.2	18.9	29.0	36.1
+ PPT [43]	ScanNet+Structured3D+S3DIS	40.7	62.0	76.9	19.4	29.4	36.8
+ SWIN3D++	ScanNet+Structured3D	41.0	62.6	77.3	21.1	32.2	38.0

Table 9. Quantitative evaluation on 3D instance segmentation.

Method	Pre.	FineTune Params.	ScanNet200			
			1%	5%	10%	20%
MaskContrast [44]	ScanNet	All	4.5	11.7	16.5	20.3
SWIN3D-S[48]	Structured3D	All	6.1	14.4	19.7	23.2
PPT [43]	ScanNet+Structured3D+S3DIS	All	6.9	14.2	19.0	22.0
SWIN3D++	ScanNet+Structured3D	All	7.6	15.2	20.7	24.2
SWIN3D++	ScanNet+Structured3D	Domain-specific	8.0	16.0	20.4	23.9

Table 10. Data efficient learning on ScanNet200 segmentation.

training data. In this setting, we only finetune the parameters related to domain-specific feature embedding, domain-specific voxel prompts, look-up tables for domain modulation, and the downsample and upsample layers, which have less than 2.5 M parameters. This finetuning strategy further improves SWIN3D++ significantly when the training data is very scarce (1% and 5%).

6. Conclusion

In this work, we addressed the challenge of integrating multiple 3D datasets with large domain discrepancies and leveraged their complementary strengths for improving 3D pretraining performance. The remarkable outcomes of SWIN3D++ attest to the benefits of multi-dataset pretraining and suggest more effective ways to utilize diverse 3D data. For future work, we intend to extend our method to multi-source outdoor datasets, which exhibit greater domain variety, complexity, and data scale.

References

- [1] Iro Armeni, Ozan Sener, Amir Roshan Zamir, Helen Jiang, Ioannis K. Brilakis, Martin Fischer, and Silvio Savarese. 3D semantic parsing of large-scale indoor spaces. In *CVPR*, 2016. 3
- [2] Hangbo Bao, Li Dong, Songhao Piao, and Furu Wei. BEiT: BERT pre-training of image transformers. In *ICLR*, 2022. 2
- [3] Shai Ben-David, John Blitzer, Koby Crammer, Alex Kulesza, Fernando Pereira, and Jennifer Wortman Vaughan. A theory of learning from different domains. *Machine learning*, 79:151–175, 2010. 3
- [4] Angel X. Chang, Thomas Funkhouser, Leonidas Guibas, Pat Hanrahan, Qixing Huang, Zimo Li, Silvio Savarese, Manolis Savva, Shuran Song, Hao Su, Jianxiong Xiao, Li Yi, and Fisher Yu. ShapeNet: An information-rich 3D model repository. arXiv:1512.03012 [cs.GR], 2015. 2
- [5] Woong-Gi Chang, Tackgeun You, Seonguk Seo, Suha Kwak, and Bohyung Han. Domain-specific batch normalization for unsupervised domain adaptation. In *CVPR*, pages 7354–7362, 2019. 2
- [6] Anpei Chen, Zexiang Xu, Andreas Geiger, Jingyi Yu, and Hao Su. TensorRF: Tensorial radiance fields. In *ECCV*, 2022. 7
- [7] Yukang Chen, Jianhui Liu, Xiaojuan Qi, Xiangyu Zhang, Jian Sun, and Jiaya Jia. LargeKernel3D: Scaling up kernels in 3D CNNs. In *CVPR*, 2023. 10
- [8] Christopher Choy, JunYoung Gwak, and Silvio Savarese. 4D spatio-temporal ConvNets: Minkowski convolutional neural networks. In *CVPR*, 2019. 2, 3
- [9] Angela Dai, Angel X. Chang, Manolis Savva, Maciej Halber, Thomas Funkhouser, and Matthias Nießner. ScanNet: Richly-annotated 3D reconstructions of indoor scenes. In *CVPR*, 2017. 1, 2, 3, 8
- [10] Xin Deng, WengYu Zhang, Qing Ding, and XinMing Zhang. Point is a vector: A feature representation in point analysis. In *CVPR*, 2023. 10
- [11] Guofan Fan, Zekun Qi, Wenkai Shi, and Kaisheng Ma. Point-GCC: Universal self-supervised 3D scene pre-training via geometry-color contrast. arXiv:2305.19623, 2023. 11
- [12] Benjamin Graham, Martin Engelcke, and Laurens van der Maaten. 3D semantic segmentation with sub-manifold sparse convolutional networks. In *CVPR*, 2018. 2
- [13] Meng-Hao Guo, Jun-Xiong Cai, Zheng-Ning Liu, Tai-Jiang Mu, Ralph R Martin, and Shi-Min Hu. PCT: Point cloud transformer. *Computational Visual Media*, 7(2):187–199, 2021. 2
- [14] Kaiming He, Xinlei Chen, Saining Xie, Yanghao Li, Piotr Dollár, and Ross B. Girshick. Masked autoencoders are scalable vision learners. In *CVPR*, pages 15979–15988, 2022. 2
- [15] Ji Hou, Benjamin Graham, Matthias Nießner, and Saining Xie. Exploring data-efficient 3D scene under-

- standing with contrastive scene contexts. In *CVPR*, 2021. 2, 10, 11
- [16] Lei Huang, Jie Qin, Yi Zhou, Fan Zhu, Li Liu, and Ling Shao. Normalization techniques in training DNNs: Methodology, analysis and application. *IEEE Trans. Pattern Anal. Mach. Intell.*, 2023. 2
- [17] Li Jiang, Hengshuang Zhao, Shaoshuai Shi, Shu Liu, Chi-Wing Fu, and Jiaya Jia. PointGroup: Dual-set point grouping for 3D instance segmentation. In *CVPR*, pages 4867–4876, 2020. 11, 12
- [18] Sebastian Koch, Albert Matveev, Zhongshi Jiang, Francis Williams, Alexey Artemov, Evgeny Burnaev, Marc Alexa, Denis Zorin, and Daniele Panozzo. ABC: A big CAD model dataset for geometric deep learning. In *CVPR*, 2019. 2
- [19] Maxim Kolodiazny, Anna Vorontsova, Anton Konushin, and Danila Rukhovich. OneFormer3D: One transformer for unified point cloud segmentation. arXiv:2311.14405, 2023. 10
- [20] Xin Lai, Jianhui Liu, Li Jiang, Liwei Wang, Hengshuang Zhao, Shu Liu, Xiaojuan Qi, and Jiaya Jia. Stratified transformer for 3D point cloud segmentation. In *CVPR*, pages 8500–8509, 2022. 2, 5, 10
- [21] John Lambert, Zhuang Liu, Ozan Sener, James Hays, and Vladlen Koltun. MSeg: A composite dataset for multi-domain semantic segmentation. In *CVPR*, 2020. 2
- [22] Haotian Liu, Mu Cai, and Yong Jae Lee. Masked discrimination for self-supervised learning on point clouds. In *ECCV*, 2022. 2
- [23] Ze Liu, Yutong Lin, Yue Cao, Han Hu, Yixuan Wei, Zheng Zhang, Stephen Lin, and Baining Guo. Swin transformer: Hierarchical vision transformer using shifted windows. In *ICCV*, pages 10012–10022, 2021. 4
- [24] Jonathan Long, Evan Shelhamer, and Trevor Darrell. Fully convolutional models for semantic segmentation. In *CVPR*, 2015. 2
- [25] Alexey Nekrasov, Jonas Schult, Or Litany, Bastian Leibe, and Francis Engelmann. Mix3D: Out-of-context data augmentation for 3D scenes. In *3DV*, pages 116–125, 2021. 10
- [26] Yatian Pang, Wenxiao Wang, Francis E. H. Tay, W. Liu, Yonghong Tian, and Liuliang Yuan. Masked autoencoders for point cloud self-supervised learning. In *ECCV*, 2022. 2
- [27] Chungyun Park, Yoonwoo Jeong, Minsu Cho, and Jaesik Park. Fast point transformer. In *CVPR*, pages 16949–16958, 2022. 2
- [28] David Rozenberszki, Or Litany, and Angela Dai. Language-grounded indoor 3d semantic segmentation in the wild. In *ECCV*, pages 125–141, 2022. 11
- [29] Danila Rukhovich, Anna Vorontsova, and Anton Konushin. FCAF3D: Fully convolutional anchor-free 3D object detection. In *ECCV*, 2021. 11
- [30] Jonas Schult, Francis Engelmann, Alexander Hermans, Or Litany, Siyu Tang, and Bastian Leibe. Mask3D for 3D semantic instance segmentation. In *ICRA*, 2022. 12
- [31] Seonguk Seo, Yumin Suh, Dongwan Kim, Jongwoo Han, and Bohyung Han. Learning to optimize domain specific normalization with domain augmentation for domain generalization. In *ECCV*, 2020. 2, 6
- [32] Yichao Shen, Zigang Geng, Yuhui Yuan, Yutong Lin, Ze Liu, Chunyu Wang, Han Hu, Nanning Zheng, and Baining Guo. V-DETR: DETR with vertex relative position encoding for 3D object detection, 2024. 11
- [33] Johanna Wald, Armen Avetisyan, Nassir Navab, Federico Tombari, and Matthias Nießner. RIO: 3D object instance re-localization in changing indoor environments. In *ICCV*, 2019. 2
- [34] Haiyang Wang, Lihe Ding, Shaocong Dong, Shaoshuai Shi, Aoxue Li, Jianan Li, Zhenguo Li, and Liwei Wang. CAGroup3D: Class-aware grouping for 3D object detection on point clouds. In *NeurIPS*, 2022. 11
- [35] Jingdong Wang, Ke Sun, Tianheng Cheng, Borui Jiang, Chaorui Deng, Yang Zhao, Dong Liu, Yadong Mu, Mingkui Tan, Xinggang Wang, Wenyu Liu, and Bin Xiao. Deep high-resolution representation learning for visual recognition. *IEEE Trans. Pattern Anal. Mach. Intell.*, 2020. 2
- [36] Peng-Shuai Wang. OctFormer: Octree-based transformers for 3D point clouds. *ACM Trans. Graph.*, 2023. 10
- [37] Peng-Shuai Wang, Yang Liu, Yu-Xiao Guo, Chun-Yu Sun, and Xin Tong. O-CNN: Octree-based convolutional neural networks for 3D shape analysis. *ACM Trans. Graph.*, 36(4):72:1–72:11, 2017. 2
- [38] Peng-Shuai Wang, Yu-Qi Yang, Qian-Fang Zou, Zhirong Wu, Yang Liu, and Xin Tong. Unsupervised 3D learning for shape analysis via multiresolution instance discrimination. In *AAAI*, 2021. 1, 2
- [39] Qi Wang, Sheng Shi, Jiahui Li, Wuming Jiang, and Xiande Zhang. Window normalization: Enhancing point cloud understanding by unifying inconsistent point densities. arXiv:2212.02287, 2022. 10
- [40] Jiajun Wu, Chengkai Zhang, Tianfan Xue, William T. Freeman, and Joshua B. Tenenbaum. Learning a probabilistic latent space of object shapes via 3D generative-adversarial modeling. In *NeurIPS*, 2016. 2
- [41] Kan Wu, Houwen Peng, Minghao Chen, Jianlong Fu, and Hongyang Chao. Rethinking and improving relative position encoding for vision transformer. In *ICCV*, pages 10033–10041, 2021. 5, 7
- [42] Xiaoyang Wu, Yixing Lao, Li Jiang, Xihui Liu, and Hengshuang Zhao. Point Transformer V2: Grouped vector attention and partition-based pooling. In *NeurIPS*, 2022. 2, 10
- [43] Xiaoyang Wu, Zhuotao Tian, Xin Wen, Bohao Peng, Xihui Liu, Kaicheng Yu, and Hengshuang Zhao. Towards large-scale 3D representation learning with multi-dataset point prompt training. 2023. 1, 2, 5, 8, 9, 10, 11, 12
- [44] Xiaoyang Wu, Xin Wen, Xihui Liu, and Hengshuang Zhao. Masked scene contrast: A scalable framework for unsupervised 3D representation learning. In *CVPR*, pages 9415–9424, 2023. 2, 10, 11, 12

- [45] Saining Xie, Jiatao Gu, Demi Guo, Charles R Qi, Leonidas J Guibas, and Or Litany. PointContrast: Unsupervised pre-training for 3D point cloud understanding. *ECCV*, 2020. 1, 2, 10
- [46] Siming Yan, Yuqi Yang, Yuxiao Guo, Hao Pan, Pengshuai Wang, Xin Tong, Yang Liu, and Qixing Huang. 3D feature prediction for masked-autoencoder-based point cloud pretraining. 2024. 2
- [47] Yaoqing Yang, Chen Feng, Yiru Shen, and Dong Tian. FoldingNet: Point cloud auto-encoder via deep grid deformation. In *CVPR*, 2018. 2
- [48] Yu-Qi Yang, Yu-Xiao Guo, Jian-Yu Xiong, Yang Liu, Hao Pan, Peng-Shuai Wang, Xin Tong, and Baining Guo. Swin3D: A pretrained transformer backbone for 3D indoor scene understanding. *Computational Visual Media*, 2023. 1, 2, 3, 4, 8, 10, 11, 12
- [49] Xumin Yu, Lulu Tang, Yongming Rao, Tiejun Huang, Jie Zhou, and Jiwen Lu. Point-BERT: Pre-training 3D point cloud transformers with masked point modeling. In *CVPR*, pages 19313–19322, June 2022. 2
- [50] Renrui Zhang, Ziyu Guo, Peng Gao, Rongyao Fang, Bin Zhao, Dong Wang, Yu Qiao, and Hongsheng Li. Point-M2AE: Multi-scale masked autoencoders for hierarchical point cloud pre-training. In *NeurIPS*, 2022. 2
- [51] Zaiwei Zhang, Rohit Girdhar, Armand Joulin, and Ishan Misra. Self-supervised pretraining of 3D features on any point-cloud. In *ICCV*, pages 10252–10263, 2021. 10
- [52] Zaiwei Zhang, Rohit Girdhar, Armand Joulin, and Ishan Misra. Self-supervised pretraining of 3D features on any point-cloud. In *ICCV*, 2021. 1, 2
- [53] Hengshuang Zhao, Li Jiang, Jiaya Jia, Philip HS Torr, and Vladlen Koltun. Point transformer. In *ICCV*, pages 16259–16268, 2021. 2
- [54] Xiangyun Zhao, Samuel Schulter, Gaurav Sharma, Yi-Hsuan Tsai, Manmohan Chandraker, and Ying Wu. Object detection with a unified label space from multiple datasets. In *ECCV*, 2020. 2
- [55] Jia Zheng, Junfei Zhang, Jing Li, Rui Tang, Shenghua Gao, and Zihan Zhou. Structured3D: A large photo-realistic dataset for structured 3D modeling. In *ECCV*, pages 519–535, 2020. 1, 2, 3, 8
- [56] Xingyi Zhou, Vladlen Koltun, and Philipp Krähenbühl. Simple multi-dataset detection. In *CVPR*, 2022. 2
- [57] Haoyi Zhu, Honghui Yang, Xiaoyang Wu, Di Huang, Sha Zhang, Xianglong He, Tong He, Hengshuang Zhao, Chunhua Shen, Yu Qiao, et al. PonderV2: Pave the way for 3D foundation model with a universal pre-training paradigm. arXiv:2310.08586, 2023. 10